



# On the Design of Two-Dimensional Quincunx Filterbanks with Directional Vanishing Moment Based on Eigenfilter Approach

Mukund B. Nagare<sup>1,3</sup> · Bhushan D. Patil<sup>2</sup> · Raghunath S. Holambe<sup>3</sup>

Received: 16 May 2019 / Revised: 13 February 2020 / Accepted: 14 February 2020 /  
Published online: 25 February 2020  
© Springer Science+Business Media, LLC, part of Springer Nature 2020

## Abstract

This paper presents a two-dimensional (2-D) eigenfilter technique to design 2-D perfect reconstruction (PR) filterbanks with directional vanishing moment (DVM). In this paper, we first introduce the DVM constraint for 2-D directional filterbank design. The proposed DVM constraint is imposed in 2-D eigenfilter formulation to obtain maximally flat 2-D low-pass analysis filter. Then, we use this designed analysis filter in 2-D time-domain formulation of PR condition to obtain complementary low-pass synthesis filters. The PR and DVM constraints are imposed to obtain 2-D low-pass synthesis filter. It is shown that the proposed 2-D filters satisfy the PR criteria with prescribed DVM. The performance of 2-D PR filters is evaluated in image denoising application. The performance of designed filterbank is compared with well-known existing methods in terms of peak signal-to-noise ratio to validate the results.

**Keywords** Denoising · Nonseparable filterbank · Perfect reconstruction · Wavelet

---

✉ Bhushan D. Patil  
bhushandpatil@gmail.com  
Mukund B. Nagare  
nagaremukund@gmail.com  
Raghunath S. Holambe  
rsholambe@gmail.com

- <sup>1</sup> Department of Instrumentation Engineering, Ramrao Adik Institute of Technology, Mumbai, India
- <sup>2</sup> Philips Healthcare Innovation Center, Pune, India
- <sup>3</sup> Department of Instrumentation Engineering, SGGS Institute of Engineering and Technology, Nanded, India

## 1 Introduction

Finding the accurate and efficient representation of images is a fundamental problem in all image processing applications. These include feature extraction, denoising, compression, classification, etc [8]. The efficiency of presentation means the ability to extract the significant information of an image using small description. This requires sparsity, which means a large amount of visual information has to be represented by small transform coefficients. Wavelet filterbanks have proven to be a highly effective tool for such applications. It is desired to have filterbanks with perfect reconstruction (PR), better frequency selectivity and desired vanishing moments (VMs) properties. The construction of lossless compression system is possible if filters satisfy PR property. To avoid the phase distortion, it is necessary to have a filterbanks with linear phase. The VMs lead to smoother basis functions. The design of nonseparable 2-D filterbanks with all aforementioned properties is a challenging task [4].

The one dimensional (1-D) wavelet filterbanks have become popular over the last few years as it provides optimal representation for 1-D piecewise smooth signals [8]. However, this fails to explore geometric regularity which exists in many natural images. For example, natural images have built in geometric structures (line and curved singularities) which are resulted from smooth boundaries of physical objects and act as a key feature in visual information. Moreover, separable 1-D wavelets can capture only limited directional information. The directional information of image is an important feature of any image processing applications. To extract the directional features, we require a 2-D wavelet bases. The conventional 2-D wavelets are constructed by taking tensor product of existing 1-D wavelets, which also fail to explore the curved singularities.

To overcome these issues, many researchers have proposed 2-D nonseparable filterbank design techniques, such as contourlets [8], directional filterbanks [25], translational invariant directional filterbanks (TIDFB) [9] and DVM filterbanks [6]. Some of these approaches do not achieve PR condition. In order to achieve good approximation, crucial property of 1-D wavelets is to have filters with VMs [18,20]. In 2-D filter representations, the VMs term is redefined as directional vanishing moment (DVM) [6], which plays important role in analyzing the geometric structures of the images. It is known that nonseparable directional filterbanks efficiently handle the orientation and geometric information. The method proposed in [6] imposes DVM in the critically sampled directional filterbanks. Researchers show that directional information plays important role in human visual process which can be efficiently extracted by 2-D directional filterbanks. The 2-D directional filterbank is implemented via  $l$ -level tree structured decomposition that leads to  $2^l$  subbands with wedge-shaped frequency partition [8]. The formulation of directional filterbank is based on Quincunx filterbanks with fan-shaped filters. The Quincunx filterbanks can be used to split frequency spectrum of input signal into low-pass and high-pass channels using diamond-shaped filters and into horizontal and vertical channel using fan-shaped filters. Intuitively, the wedge-shaped frequency partition of the directional filterbank is realized by an appropriate combination of directional frequency splitting by the fan-shaped filters and the rotation operations done by resampling. The choice of fan-shaped filters with

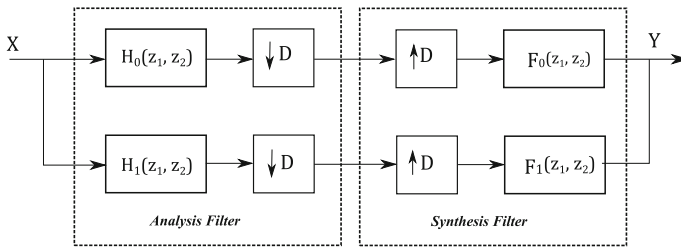


**Fig. 1** 2-D two-channel filterbank structure

sharper frequency response and directional sensitivity gives better results in computer vision, seismic signals processing and image compression applications [2,8,9].

This paper aims to design 2-D PR filterbanks which have filters with DVM. The filters are designed using 2-D eigenfilter approach (EFA). In this method, DVM and PR constraints are imposed in EFA design formulation to construct 2-D directional filters with DVM. The proposed approach is numerically efficient and linear phase constraints can be easily used in design formulation [27]. Many conventional methods of 2-D filter design have been appeared in [1,3,11,15,22,24]. These designs are based on variable transformation and optimization techniques. In commonly used transformation methods, 1-D prototype of filterbank is designed and mapped into 2-D filters through McClellan transformation [22]. The limitation of this approach is that we cannot explicitly control the shape of frequency response of 2-D filters. Moreover, these filters can achieve near PR (not complete PR). Recently, few design methods of 2-D quincunx filterbanks have been appeared in [13,16,17,21,25]. However, the filters designed by these methods do not consider the DVM property.

In this paper, we propose a method to design 2-D PR quincunx filterbank with DVM. In the proposed approach, 2-D low-pass analysis filters are designed by imposing DVM constraint in the 2-D EFA formulation. The EFA can incorporate both time-domain and frequency-domain constraints easily in the design. Therefore, the designed low-pass analysis filter and DVM constraint are used in 2-D time-domain formulation of PR condition to obtain complementary 2-D low-pass synthesis filter. We consider the fan-shaped filter design which plays an important role in the directional filterbanks. The directional filters designed by proposed eigenfilter method satisfy DVM property. This improves the regularity of proposed 2-D filters. The proposed filters satisfy PR criteria and have comparable performance to existing 2-D filters.

## 2 Preliminaries

The two-channel 2-D quincunx filterbank structure is shown in Fig. 1. Here, we use 2-D quincunx sampling which has the down-sampling ratio of 2, i.e.,  $\det(D) = 2$ . The set of filters  $H_0(z_1, z_2)$  and  $H_1(z_1, z_2)$  represent the analysis of low-pass and high-pass filters, respectively. Similarly, the set of filters  $F_0(z_1, z_2)$  and  $F_1(z_1, z_2)$  denote synthesis filters. The quincunx sampling is a nonseparable sampling, and it treats different directional information more effectively than conventional methods.

The points of quincunx sublattice at  $(n_1 + n_2 = \text{even})$  are kept unchanged, while points at  $(n_1 + n_2 = \text{odd})$  sublattice are set to zero. With these filters, the reconstructed image obtained is the perfect replica of the original image if it satisfies the following conditions

$$H_0(z_1, z_2)F_0(z_1, z_2) + H_1(z_1, z_2)F_1(z_1, z_2) = 2z_1^{-d_1}z_2^{-d_2} \quad (1)$$

where  $d$  represents delay. The alias cancellation condition can be given as

$$H_0(-z_1, -z_2)F_0(z_1, z_2) + H_1(-z_1, -z_2)F_1(z_1, z_2) = 0. \quad (2)$$

By choosing high-pass filters as  $H_1(z_1, z_2) = F_0(-z_1, -z_2)$  and  $F_1(z_1, z_2) = -H_0(-z_1, -z_2)$ , alias cancellation condition (2) satisfies. The product filter can be defined as  $P(z_1, z_2) = H_0(z_1, z_2)F_0(z_1, z_2)$  which gives

$$P(z_1, z_2) + P(-z_1, -z_2) = 2z_1^{-d_1}z_2^{-d_2} \quad (3)$$

Hence, the aim of designing a 2-D directional filterbank is the problem of designing  $P(z_1, z_2)$  by imposing the respective constraints.

### 3 Proposed Problem Formulation for Design of 2-D Two-Channel PR Filterbank

In this section, we discuss the proposed EFA with DVM constraint. We first discussed the DVM constraint imposed in two dimensions. Then, these constraints are used in proposed EFA design formulation.

#### 3.1 Directional Vanishing Moment constraints

The crucial role of wavelet in analyzing transient signal is because of the VMs or regularity properties of wavelets. The wavelet properties, such as time localization and VMs, give the sparse representation for piecewise polynomial signals. Majority of the earlier wavelet filters like Daubechies wavelet filters, and JPEG2000 filters have been designed by considering VMs as a first criterion. The VMs can be characterized by imposing zeros in low-pass and high-pass filters of given filterbank.

Consider a 2-D FIR filter  $(h_0(n_1, n_2))$  with quadrantal symmetry, which have 2-D support of  $-N_1 < n_1 < N_1$ , and  $-N_2 < n_2 < N_2$ . The filter response  $H_0(\omega_1, \omega_2)$  of the linear phase filter can be expressed as

$$H_0(\omega_1, \omega_2) = \sum_{n_1=0}^{\frac{N_1-1}{2}} \sum_{n_2=0}^{\frac{N_2-1}{2}} h(n_1, n_2) \cos(n_1\omega_1) \cos(n_2\omega_2). \quad (4)$$

Assume that  $H_0(z)$  is the 1-D low-pass filter of analysis filterbanks. This filter is said  $k$  regular if it has  $k$  number of zeros at location  $z = -1$  or  $\omega = \pi$  on the unit circle. For

2-D filterbanks, the VMs condition requires the low-pass filter to have  $L$ th-order zero derivatives that mean zeros at  $[z_1, z_2] = [-1, -1]$  or  $[\omega_1, \omega_2] = [\pi, \pi]$ . Therefore, partial derivative of  $H_0(\omega_1, \omega_2)$  is given by

$$\frac{\partial^{l_0+l_1} H_0}{\partial \omega_0^{l_0} \partial \omega_1^{l_1}} = \begin{cases} \sum_{n_1=-N_1}^{N_1} \sum_{n_2=-N_2}^{N_2} h_0(n_1, n_2) (n_1)^{l_0} (n_2)^{l_1} \cos(n_1 \omega_1) \cos(n_2 \omega_2), & \text{for } L = \text{even} \\ - \sum_{n_1=-N_1}^{N_1} \sum_{n_2=-N_2}^{N_2} h_0(n_1, n_2) (n_1)^{l_0} (n_2)^{l_1} \sin(n_1 \omega_1) \sin(n_2 \omega_2) & \text{otherwise} \end{cases} \tag{5}$$

where,  $L = [l_0, l_1]^T \in \mathbb{Z}^2$  (set of integer values). From above equation, it follows that when,  $L \in \mathbb{Z}_o$  (i.e., set of odd integer values), the  $L$ th-order partial derivative of  $H_0(\omega_1, \omega_2)$  is automatically zero at  $[\omega_1, \omega_2] = [\pi, \pi]$ . If  $L$ th order zeros are imposed at  $[z_1, z_2] = [-1, -1]$  on low-pass filter, then the impulse response  $h_0(n_1, n_2)$  must satisfy the condition given by

$$\sum_{n_1=-N_1}^{N_1} \sum_{n_2=-N_2}^{N_2} (n_1)^{l_0} (n_2)^{l_1} (-1)^{n_1} (-1)^{n_2} h_0(n_1, n_2) = 0, \tag{6}$$

for  $l_0 = 0, 1, \dots, 2v_1 - 1$  and  $l_1 = 0, 1, \dots, 2v_2 - 1$

Since  $h_0(n_1, n_2)$  is a zero-phase filter, the above condition is rewritten as,

$$\begin{cases} h_0(0, 0) + 2 \sum_0^{N_1} \sum_0^{N_2} (-1)^{n_1} (-1)^{n_2} h_0(n_1, n_2) = 0 \\ 2 \sum_0^{N_1} \sum_0^{N_2} (n_1)^{l_0} (n_2)^{l_1} (-1)^{n_1} (-1)^{n_2} h_0(n_1, n_2) = 0 \end{cases} \tag{7}$$

for  $l_0 = 0, 1, \dots, 2v_1 - 1$  and  $l_1 = 0, 1, \dots, 2v_2 - 1$

In this design, DVM constraint is formulated in time matrix form as  $\mathbf{\Gamma} \hat{\mathbf{b}} = 0$ , where vector  $\hat{\mathbf{b}} \in \mathbb{R}^{(N+1) \times (N+1)}$  which contains filter coefficients  $h_0(n_1, n_2)$  and  $\mathbf{\Gamma} \in \mathbb{R}^{(L) \times (N+1)}$ . It is given by

$$\mathbf{\Gamma}_{L,n} = \begin{cases} 1 & n_1 = 0, \quad n_2 = 0 \\ 2(n_1)^{l_0} (n_2)^{l_1} (-1)^{n_1} (-1)^{n_2} = 0 \end{cases} \tag{8}$$

for  $l_0 = 1, \dots, 2v_1 - 1$  and  $l_1 = 1, \dots, 2v_2 - 1$

This matrix is used as a DVM constraint in the EFA problem to design low-pass and high-pass filters. The linear function of error between passband and stopband is minimized subject to DVM constraints in EFA.

### 3.2 Design of Analysis Low-pass Filter with DVM Using EFA

In this section, the 2-D EFA is proposed to design 2-D analysis low-pass filter with DVM constraint. Consider a 2-D FIR filter given in equation (4). The frequency response of quadrantal symmetric filter can be given as

$$H_0(\omega_1, \omega_2) = \sum_{n_1=0}^{N_1-1} \sum_{n_2=0}^{N_2-1} a(n_1, n_2)\cos(n_1\omega_1)\cos(n_2\omega_2) \tag{9}$$

where  $H_0(\omega_1, \omega_2)$  is a frequency response to be obtained and  $a(n_1, n_2)$  are the coefficients related to filter impulse response  $h_0[n_1, n_2]$  with quadrantal symmetry. Assume,  $N_1 = N_2 = N$  and defining column vectors  $\mathbf{a}$  and  $\hat{\mathbf{c}}(\omega_1, \omega_2)$  as

$$\mathbf{a} = [a(0, 0), a(0, 1), \dots, a(0, N_2) | a(1, 0), \dots, a(1, N_2) | \dots | a(N_1, 0), \dots, a(N_1, N_2)]^T \tag{10}$$

$$\hat{\mathbf{c}} = [1, \cos(\omega_2), \dots, \cos((N_2 - 1)\omega_2) | \cos(\omega_1), \cos(\omega_1).\cos(\omega_2), \dots, \cos(\omega_1).\cos((N_2 - 1)\omega_2) | \cos((N_1 - 1)\omega_1, \cos((N_1 - 1)\omega_1).\cos(\omega_2), \dots, \cos((N_1 - 1)\omega_1)\cos((N_2 - 1)\omega_2)]^T \tag{11}$$

The frequency response for the filter  $H_0(\omega_1, \omega_2)$  can be written in vector form as

$$H_0(\omega_1, \omega_2) = \mathbf{a}^T . \hat{\mathbf{c}}(\omega_1, \omega_2) \tag{12}$$

The objective of the eigenfilter method is to minimize the quadratic measure between the passband error function  $\xi_p$  and stopband error function  $\xi_s$  of the filter. This can be formulated as

$$\begin{aligned} \xi &= \alpha \xi_p + \beta \xi_s \text{ where} \\ \xi_p &= \frac{1}{(2\pi)^M} \iint_{passband \in \mathcal{R}} [H_D(\omega_{ref}) - H_0(\omega_1, \omega_2)]^2 d\omega_1 d\omega_2 \\ \xi_s &= \frac{1}{(2\pi)^M} \iint_{stopband \in \mathcal{R}} [H_0(\omega_1, \omega_2)]^2 d\omega_1 d\omega_2. \end{aligned} \tag{13}$$

where,  $H_D(\omega_1, \omega_2)$  is the ideal frequency response and  $H_0(\omega_1, \omega_2)$  is a frequency response of 2-D filter which is to be obtained. The  $\alpha, \beta$  are the constants and control the approximation of accuracies in the passband and stopband. The main objective is to minimize the error function. This error function can be written as  $\xi = \mathbf{a}^T \mathbf{R}_1 \mathbf{a}$ , where  $\mathbf{a}$  denotes the real vector, while  $\mathbf{R}_1$  represents real, symmetric and positive definite matrix. Here, the objective is to find the vector  $\mathbf{a}$ . The elements of vector  $\mathbf{a}$  correspond to the 2-D filter impulse response  $h_0[n_1, n_2]$ .

Thus, the passband and stopband error function can be evaluated as  $\xi_p = \mathbf{a}^T \mathbf{R}_p \mathbf{a}$  and  $\xi_s = \mathbf{a}^T \mathbf{R}_s \mathbf{a}$ , with

$$\mathbf{R}_p = \frac{1}{(2\pi)^M} \iint_{\text{passband} \in \mathcal{R}} [\hat{\mathbf{c}}(\omega_{ref}) - \hat{\mathbf{c}}(\omega_1, \omega_2)] \times [\hat{\mathbf{c}}(\omega_{ref}) - \hat{\mathbf{c}}(\omega_1, \omega_2)]^T d\omega_1 d\omega_2$$

and

$$\mathbf{R}_s = \frac{1}{(2\pi)^M} \iint_{\text{stopband} \in \mathcal{R}} [\hat{\mathbf{c}}(\omega_1, \omega_2)] [\hat{\mathbf{c}}(\omega_1, \omega_2)]^T d\omega_1 d\omega_2$$

where  $\omega_{ref}$  denotes the reference frequency of passband region. The total error function to be minimized in (13) can be expressed as

$$\xi = \alpha \xi_p + \beta \xi_s = \mathbf{a}^T \mathbf{R}_1 \mathbf{a}, \text{ where } \mathbf{R}_1 = \alpha \mathbf{R}_p + \beta \mathbf{R}_s. \quad (14)$$

Here,  $\mathbf{R}_1$  represents the real, symmetric and positive definite matrix. Here, the aim is not only to satisfy the objective of minimum error function but also to satisfy the DVM constraints given in Eq. (8). Thus, this design can be casted as constrained optimization problem as:

$$\begin{aligned} & \underset{\xi}{\text{minimize}} \quad \xi = \mathbf{h}^T \mathbf{R}_1 \mathbf{h} \\ & \text{subject to} \quad \mathbf{\Gamma} \mathbf{h} = \mathbf{0} \text{ and } \mathbf{h}^T \mathbf{h} = 1. \end{aligned} \quad (15)$$

Using Rayleigh principle [27], eigenvector of  $\mathbf{R}_1$  which corresponds to minimum eigenvalue gives minimum  $\xi$ . The DVM constraints are imposed in the form of  $\mathbf{\Gamma} \mathbf{h} = \mathbf{0}$  as described by pei et al. in [23]. To solve this constrained optimization problem, we note that  $\mathbf{\Gamma} \mathbf{h} = \mathbf{0}$  if and only if  $\mathbf{h}$  spans the null space of  $\mathbf{\Gamma}$ . Therefore, any such vector which satisfies the constraints can be expressed as  $\mathbf{h} = \mathbf{U} \mathbf{b}$ , where columns of  $\mathbf{U}$  form an orthogonal to basis for null space of the matrix  $\mathbf{\Gamma}$ . Note that  $\mathbf{U}$  is a unitary matrix, i.e.,  $\mathbf{U}^T \mathbf{U} = \mathbf{I}$  and  $\mathbf{b}$  is any arbitrary vector. With this modification of  $\mathbf{h}$ , the design problem becomes

$$\underset{\xi}{\text{minimize}} \quad \xi = \mathbf{h}^T \mathbf{R}_1 \mathbf{h} = \mathbf{b}^T \mathbf{U}^T \mathbf{R}_1 \mathbf{U} \mathbf{b}. \quad (16)$$

Therefore, the eigenvector of  $\mathbf{U}^T \mathbf{R}_1 \mathbf{U}$  corresponding to minimum eigenvalue yield minimum passband and stopband error. Singular value decomposition (SVD) is used to find the eigenvalue and eigenvector. The optimal solution  $\mathbf{h}$  is equal to  $\mathbf{U} \mathbf{b}$ . The elements of this vector represent the coefficients of analysis low-pass filter with prescribed DVM.

### 3.3 Design of Synthesis Low-Pass Filter with PR and DVM constraints Using EFA

The coefficient of polynomial  $H_0(z_1, z_2)$  is elements of eigenvector of  $U^T R_1 U$  corresponding to minimum eigenvalue. The coefficients of polynomial  $F_0(z_1, z_2)$  are obtained using Eq. (3) and the coefficient of polynomial  $P_0(z_1, z_2)$ . Assume that  $h_0(n_1, n_2)$  and  $f_0(n_1, n_2)$  are the zero-phase filters with 2-D support as

$$\begin{aligned} h_0[n_1, n_2] &= \text{nonzero for } -P \leq n_1, n_2 \leq P \\ f_0[n_1, n_2] &= \text{nonzero for } -Q \leq n_1, n_2 \leq Q. \end{aligned}$$

Note that in time domain,  $p[n_1, n_2]$  is the 2-D convolution of  $h_0[n_1, n_2]$  and  $f_0[n_1, n_2]$  as given below:

$$\begin{aligned} p[n_1, n_2] &= \sum_{k_1=-Q}^Q \sum_{k_2=-Q}^Q f_0[k_1, k_2] \cdot (h_0[n_1 - k_1, n_2 - k_2]) \\ &\text{for } -(P + Q) \leq n_1, n_2 \leq (P + Q). \end{aligned} \tag{17}$$

Since  $f_0[n_1, n_2]$  is zero phase,  $f_0[n_1, n_2] = f_0[-n_1, -n_2]$ . For zero-phase filter,  $f_0[n_1, n_2]$  with centro-symmetry has the following number of independent coefficients

$$\left( \begin{array}{l} f_0[0, n_2], 0 \leq n_2 \leq Q \\ f_0[n_1, n_2], 1 \leq n_1 \leq Q, -Q \leq n_2 \leq Q \end{array} \right). \tag{18}$$

Therefore, Eq. (17) can be rewritten using independent coefficients of  $f_0[n_1, n_2]$  as follows:

$$\begin{aligned} p[n_1, n_2] &= f_0[0, 0] \cdot h_0[n_1, n_2] + \sum_{k_2=1}^Q f_0[0, k_2] \cdot (h_0[n_1, n_2 - k_2] + h_0[n_1, n_2 + k_2]) \\ &+ \sum_{k_1=1}^Q \sum_{k_2=-Q}^Q f_0[k_1, k_2] \cdot (h_0[n_1 - k_1, n_2 - k_2] + h_0[n_1 + k_1, n_2 + k_2]) \\ &\text{for } -(P + Q) \leq n_1, n_2 \leq (P + Q). \end{aligned} \tag{19}$$

Note that  $h_0[n_1, n_2]$  and  $f_0[n_1, n_2]$  are zero phase, which follows that  $p_0[n_1, n_2]$  is also zero phase, i.e.,  $p_0[n_1, n_2] = p_0[-n_1, -n_2]$ . To achieve PR, product filter must satisfy

$$\begin{aligned} p[n_1, n_2] &= 1 && \text{for } n_1 = n_2 = 0 \\ p[n_1, n_2] &= 0 && \text{otherwise} \end{aligned} \tag{20}$$



This expresses  $p[n_1, n_2] = 0$  for all samples on quincunx locations and represented by  $N_L$ . Then,

$$N_L = \frac{N-1}{2} + \left\lfloor \frac{N \cdot (2N+1)}{2} \right\rfloor, \text{ when } N = \text{odd integer}$$

$$N_L = \frac{N}{2} + \frac{N \cdot (2N+1)}{2}, \text{ when } N = \text{even integer}$$

Thus, from (19) and (20), it is noted that we can solve  $N_L + 1$  equations for  $2Q^2 + 2Q + 1$  number of unknown variables. This corresponds to independent coefficients of  $f_0[n_1, n_2]$ . Similar to analysis filter design, we impose PR and DVM constraints to obtain low-pass synthesis coefficients. The independent coefficients  $f_0[n_1, n_2]$  are arranged in vector  $\mathbf{f}$ . Therefore, Eq. (19) is rewritten as

$$\mathbf{C}\mathbf{f} = \mathbf{d}, \quad (21)$$

where  $\mathbf{C}$  is the matrix of size  $(N_L + 1) \times (2Q^2 + 2Q + 1)$  and is obtained from Eq. (19). The vector  $\mathbf{f}$  contains the unknown coefficients of  $f_0[n_1, n_2]$  of size  $(2Q^2 + 2Q + 1) \times 1$  and  $\mathbf{d} = [1 \ 0 \ \dots \ 0]^T$ . Equation (21) gives multiple solutions but goal is to find one optimal solution. So, constraints are rewritten as

$$\hat{\mathbf{C}}\mathbf{f} = 0 \quad \text{where } \hat{\mathbf{C}} = \mathbf{C} - \frac{\mathbf{d} \cdot \hat{\mathbf{c}}^t(\omega_0)}{H_D(\omega_0)} \quad (22)$$

Here,  $\hat{\mathbf{c}}^t(\omega_0)$  matrix and  $H_D(\omega_0)$  are related to equivalent form of the zero reference frequency condition (refer [27]). Hence, 2-D filter design problem becomes constrained (DVM and PR) optimization problem as

$$\begin{aligned} &\text{minimize } \xi = \mathbf{f}^T \mathbf{R}_2 \mathbf{f} \\ &\quad \xi \\ &\text{subject to } \mathbf{\Gamma} \mathbf{f} = \mathbf{0}, \quad \hat{\mathbf{C}} \mathbf{f} = \mathbf{0} \text{ and } \mathbf{f}^T \mathbf{f} = \mathbf{1}. \end{aligned} \quad (23)$$

Here,  $\mathbf{R}_2$  represents the real, symmetric and positive definite matrix. To solve this constrained optimization problem, we note that  $\mathbf{\Gamma} \mathbf{f} = \mathbf{0}$  if and only if  $\mathbf{f}$  spans the null space of  $\mathbf{\Gamma}$ . Therefore, any such vector which satisfies the constraints can be expressed as  $\mathbf{f} = \mathbf{U}\mathbf{b}$ , where columns of  $\mathbf{U}$  form an orthogonal to basis for null space of the matrix  $\mathbf{\Gamma}$ . Note that  $\mathbf{U}$  is a unitary matrix, i.e.,  $\mathbf{U}^T \mathbf{U} = \mathbf{I}$  and  $\mathbf{b}$  is any arbitrary vector. The objective function is minimized with PR (22) and DVM constraints (8).

This can be expressed as  $\xi = \mathbf{b}^T \mathbf{U}^T \mathbf{R}_2 \mathbf{U} \mathbf{b}$ . The optimal solution  $\mathbf{b}$  of this error function is the eigenvector of the matrix  $\mathbf{U}^T \mathbf{R}_2 \mathbf{U}$ . This eigenvector is corresponding to minimum eigenvalue of the matrix  $\mathbf{R}_2$ . Finally, the optimal solution  $\mathbf{f}$  is equal to  $\mathbf{U}\mathbf{b}$ . The elements of this vector represent the coefficients of synthesis low-pass filter  $f_0[n_1, n_2]$ .

Design example: To design 2-D fan-shaped analysis low-pass filter  $h_0(n_1, n_2)$ , we consider  $\omega_{p1}$ ,  $\omega_{p2}$  and  $\omega_{s1}$ ,  $\omega_{s2}$  which describe the passband and stopband cut-off

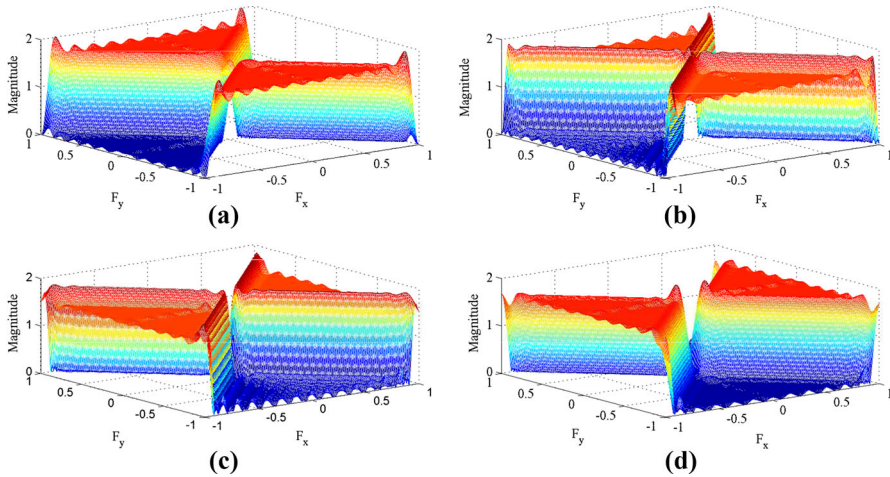


**Fig. 2** Frequency response of the proposed fan-shaped analysis filters and synthesis filters

frequencies. We consider the low-pass filter size  $N_1 = N_2 = 23$ ,  $\omega_{p1} = \omega_{p2} = 0.4\pi$ ,  $\omega_{s1} = \omega_{s2} = 0.6\pi$ ,  $\alpha = \beta = 0.5$  and  $\omega_{ref} = (0, 0)$ . For this  $h_0(n_1, n_2)$ , we design corresponding synthesis filter  $f_0(n_1, n_2)$  with  $Q = 25$ . The analysis low-pass filter  $h_0(n_1, n_2)$  is quadrantal symmetric and its first quadrant coefficients denoted by  $h_I$  are given in Eq. (24), where, its center value is  $-0.8158$ . The frequency response of the proposed 2-D filters is shown in Fig. 2.

$$h_I = \begin{bmatrix} 0 & -0.0023 & 0 & -0.0022 & 0 & -0.0021 & 0 & -0.0019 & 0 & -0.0016 & 0 & -0.0015 \\ -0.0041 & 0 & -0.00025 & 0 & -0.0015 & 0 & -0.0015 & 0 & -0.0013 & 0 & -0.0012 & 0 \\ 0 & -0.0069 & 0 & 0.0027 & 0 & -0.00024 & 0 & -0.00057 & 0 & -0.00053 & 0 & -0.00049 \\ -0.0043 & 0 & -0.01041 & 0 & 0.0069 & 0 & 0.0015 & 0 & 0.00076 & 0 & 0.00061 & 0 \\ 0 & -0.0057 & 0 & -0.0146 & 0 & 0.0123 & 0 & 0.0039 & 0 & 0.0026 & 0 & 0.0023 \\ -0.0044 & 0 & -0.0072 & 0 & -0.0197 & 0 & 0.0193 & 0 & 0.0071 & 0 & 0.0052 & 0 \\ 0 & -0.0054 & 0 & -0.0089 & 0 & -0.0262 & 0 & 0.0286 & 0 & 0.0116 & 0 & 0.0096 \\ -0.0043 & 0 & -0.0065 & 0 & -0.0109 & 0 & -0.0347 & 0 & 0.0417 & 0 & 0.01898 & 0 \\ 0 & -0.0051 & 0 & -0.0078 & 0 & -0.0136 & 0 & -0.0472 & 0 & 0.0636 & 0 & 0.0349 \\ -0.0042 & 0 & -0.0061 & 0 & -0.0093 & 0 & -0.0174 & 0 & -0.0683 & 0 & 0.1117 & 0 \\ 0 & -0.0050 & 0 & -0.0073 & 0 & -0.0115 & 0 & -0.0242 & 0 & -0.1159 & 0 & 0.3449 \\ -0.0041 & 0 & -0.0060 & 0 & -0.0089 & 0 & -0.0153 & 0 & -0.03962 & 0 & -0.3488 & -0.8158 \end{bmatrix} \tag{24}$$

### 4 Experimental Results

To illustrate the effectiveness of the proposed filter with DVM, we have carried out experiments on image denoising application.

#### 4.1 Image Denoising

The performance of the designed filters has been tested in the denoising application. Image denoising is an exemplary issue and has been studied for a long time. However, it remains a challenging and open task. The brief review of recently appeared denoising techniques has been studied in [10]. In general, image denoising techniques are

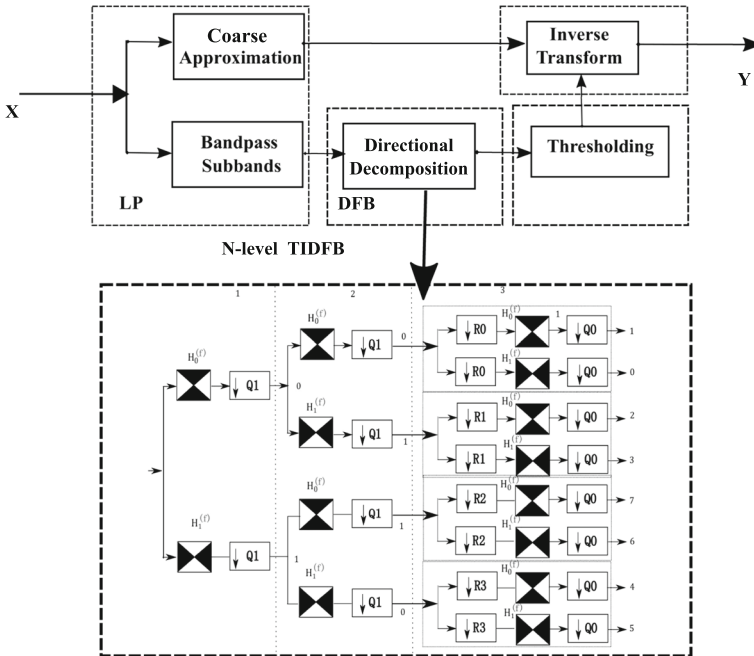


**Fig. 3** Denoising scheme using directional filterbank with proposed filters

classified as spatial domain and transform domain methods. The aim of spatial domain methods is to remove noise by calculating the gray value of each pixel based on the correlation between pixels/image patches in the original image [14]. Furthermore, spatial domain methods can be divided into two categories, namely spatial domain filtering and variational denoising methods. However, transform domain filtering methods first transform the given noisy image to another domain, and then they apply a denoising procedure on the transformed image according to the different characteristics of the image and its noise. The larger coefficients represent the high-frequency part, i.e., the details or edges of the image and smaller coefficients represents the noise. Initially, transform domain methods were developed from the Fourier transform, but since then, a variety of transform domain methods gradually emerged, such as wavelet domain methods [29], and block-matching and 3-D filtering (BM3D) [7]. Recently, CNN-based methods have been developed rapidly and have performed well in many computer vision tasks [12,19]. The use of a CNN for image denoising can be tracked back, where a five-layer network was developed. In recent years, many CNN-based denoising methods have been proposed [5,28].

The proposed filters are used in denoising scheme as shown in Fig. 3. The denoising scheme mainly consists of two stages: a Laplacian pyramid (LP) decomposition [8] and directional filterbank (DFB) decomposition. The proposed filters are used in directional decomposition as shown in Fig. 3. Laplacian pyramid decomposes the standard images (e.g., Barbara ( $512 \times 512$ )) into approximation information and radial bandpass subbands with different directional information. Then, DFB is applied to each

**Table 1** SNR and PSNR values of the denoising experiments (values are in dB)

Image	$\sigma$	Noisy		CT [8]		CTSD [8]		TIWT [9]		STICT [9]		TICT [9]		BM3D [7]		Proposed	
		PSNR	SNR	PSNR	SNR	PSNR	SNR	PSNR	SNR	PSNR	SNR	PSNR	SNR	PSNR	SNR	PSNR	SNR
Barbara	10	28.13	26.38	29.27	28.51	31.40	29.19	32.52	29.81	33.16	30.12	33.46	32.09	34.98	31.58	35.06	
	20	22.11	23.13	26.027	25.46	28.30	24.84	28.22	25.84	29.22	26.10	29.48	28.89	31.78	28.25	31.08	
	30	18.57	21.39	24.25	23.64	26.56	22.47	25.89	23.52	26.97	23.8	27.26	26.92	29.81	25.76	28.86	
	40	16.08	20.24	23.16	22.33	25.21	21.15	24.50	22.03	25.41	22.31	25.68	25.09	27.99	25.02	28.28	
	50	14.13	19.39	22.24	21.43	24.30	20.10	23.58	20.75	24.31	21.02	24.59	24.32	27.23	22.03	25.78	
	60	12.56	18.77	21.65	20.71	23.58	19.35	22.83	19.88	23.34	20.15	23.60	23.37	26.28	21.07	24.02	
Lena	10	28.11	28.96	31.66	31.38	34.03	31.89	34.56	32.02	34.69	32.24	34.91	33.25	35.91	33.44	36.21	
	20	22.10	26.005	28.59	28.79	31.40	28.63	31.34	28.78	31.50	29.03	31.72	30.38	33.05	31.58	33.01	
	30	18.60	24.29	26.88	27.5	29.72	26.69	29.43	26.83	29.53	27.03	29.78	28.60	31.26	29.84	31.08	
	40	16.05	22.93	25.63	25.73	28.44	25.15	27.87	25.25	27.96	25.56	28.26	27.21	29.86	28.26	29.36	
	50	14.15	22.01	24.54	24.75	27.30	23.83	26.58	23.89	26.86	24.19	26.91	26.39	29.05	25.36	28.21	
	60	12.58	21.24	23.78	23.88	26.49	22.68	25.49	22.70	25.47	23.04	25.80	25.60	28.27	24.33	27.01	
70	11.25	20.64	23.05	23.29	25.81	21.91	24.50	21.81	24.50	22.12	24.81	24.90	27.57	23.31	26.11		

Table 1 continued

Image	$\sigma$	Noisy		CT [8]		CTSD [8]		TIWT [9]		STICT [9]		TICT [9]		BM3D [7]		Proposed	
		PSNR	SNR	PSNR	SNR	PSNR	SNR	PSNR	SNR	PSNR	SNR	PSNR	SNR	PSNR	SNR	PSNR	SNR
Peppers	10	28.11	27.42	31.007	29.37	33.002	29.19	33.93	29.81	33.84	30.12	34.03	31.47	34.68	30.75	34.75	
	20	22.10	24.64	28.26	27.19	30.84	29.15	30.98	29.73	30.93	30.04	31.17	29.18	31.29	29.52	31.89	
	30	18.58	22.89	26.48	25.64	29.17	22.50	28.80	23.53	28.75	23.81	29.03	27.65	29.28	24.58	29.75	
	40	16.04	21.53	25.20	24.36	27.99	22.53	27.04	23.61	27.004	23.88	27.28	26.36	27.7	24.55	28	
	50	14.12	20.54	24.16	23.28	27.51	21.06	25.60	21.93	25.55	22.19	25.84	25.51	26.68	22.80	26.56	
	60	12.57	19.75	23.38	22.49	26.048	19.38	24.33	19.87	24.22	20.15	24.49	24.70	25.81	20.83	25.21	
	70	11.23	19.06	22.72	21.73	25.44	18.75	23.29	19.12	23.20	19.37	23.45	23.97	25.07	18.87	24.17	
Boats	10	28.12	28.41	30.26	30.57	32.41	29.16	33.31	29.78	33.30	30.08	33.57	33.27	33.92	30.64	34.2	
	20	22.13	25.28	27.11	27.62	29.51	24.83	29.73	25.84	29.75	26.11	30.31	29.84	30.88	26.84	31.16	
	30	28.59	23.57	25.43	25.91	27.78	22.51	27.70	23.62	27.66	23.90	27.90	27.89	29.12	25.18	29.4	
	40	16.09	24.73	24.39	22.53	26.67	21.09	26.30	22.03	26.22	22.30	26.46	28.45	27.74	23.61	28.02	
	50	14.13	21.66	23.57	23.83	25.74	20.13	25.19	20.77	25.09	21.05	25.32	25.49	26.78	21.28	25.6	
	60	12.56	20.93	22.71	23.09	24.97	19.34	24.14	19.85	23.99	20.10	24.11	24.70	26.02	20.32	25	
	70	11.23	20.23	22.19	22.39	24.39	18.74	23.27	19.06	23.11	19.31	23.34	24.04	25.4	19.68	23.62	



**Fig. 4** Denoising results of Barbara image **a** noisy image  $\sigma = 20$  **b** denoised image with CT **c** CTSD **d** TIWT **e** STICT **f** TICT **g** BM3D **h** Proposed Method

radial bandpass subbands where maximum fine structural details of Barbara image for different directions are extracted efficiently. The DFB in second step can be implemented by using tree structured decomposition. In these experiments, the images are decomposed upto three-level ( $N = 3$ ) directional decomposition. The subband images of DFB are decimated by the following subsampling matrices

$$\begin{aligned}
 Q_0 &= \begin{bmatrix} 1 & -1 \\ 1 & 1 \end{bmatrix} & Q_1 &= \begin{bmatrix} 1 & 1 \\ -1 & 1 \end{bmatrix} & R_0 &= \begin{bmatrix} 1 & 1 \\ 0 & 1 \end{bmatrix} \\
 R_1 &= \begin{bmatrix} 1 & -1 \\ 0 & 1 \end{bmatrix} & R_2 &= \begin{bmatrix} 1 & 0 \\ -1 & 1 \end{bmatrix} & R_3 &= \begin{bmatrix} 1 & 0 \\ 1 & 1 \end{bmatrix}.
 \end{aligned} \tag{25}$$

Noise generally contained high-frequency component due to which it lies in the high-frequency subbands. Therefore, we threshold the detail subbands to suppress the noise content present in the image and reconstruct the original image. The noise is suppressed using hard thresholding, and it is estimated by using Bayes' shrinkage rule. We have tested the performance of designed 2-D filters on four standard commonly used images, such as Lena ( $512 \times 512$ ), Peppers ( $512 \times 512$ ), Boat ( $512 \times 512$ ) and Barbara ( $512 \times 512$ ) [26]. The test images are contaminated first by adding a zero-mean Gaussian white noise with a standard deviation of  $\sigma$ . For all the denoising schemes, we assumed that  $\sigma$  is unknown, and we estimated it using the robust median estimator as given in [9]. These noisy images are then used in the denoising scheme. The denoising performance of the proposed filters is compared with the existing well-known methods, such as 1-D wavelets [20], Contourlet transform (CT) [8], ContourletSD [8], TIWT [9], STICT [9], TICT [9] and BM3D [7]. The conventional 'PKVA' filters have been used in the CT [8] and TICT [9] methods. In order to obtain an insightful analysis, the qualitative objective measures, such as signal-to-noise ratio (SNR), peak signal-to-

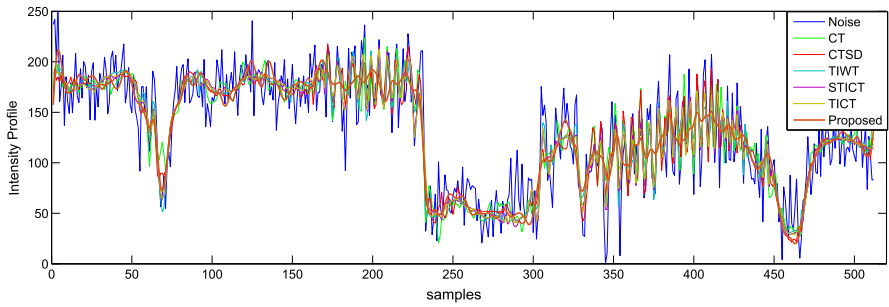


**Fig. 5** Comparison of relative intensity profiles of denoised image with known methods for Barbara (512 × 512) image

**Table 2** Energy distribution of first subband

Method	TIWT [9]	STICT [9]	TICT [9]	Proposed
Energy	4.81e9	2.38e9	5.81e9	3.061e10

noise ratio (PSNR) are measured. PSNR is commonly used to measure the distortion. For an original image  $X$  and its reconstructed version  $Y$ , the PSNR is defined as

$$PSNR = 20 \log_{10} \left( \frac{2^P - 1}{\sqrt{MSE}} \right) \tag{26}$$

where

$$MSE = \frac{1}{N_0 N_1} \sum_{i_0}^{N_0-1} \sum_{j_0}^{N_1-1} [Y(i_0, j_0) - X(i_0, j_0)]^2, \tag{27}$$

and each image has  $P$  bits/sample and dimension  $N_0 \times N_1$ .

Table 1 depicts the SNR and PSNR values of denoising results obtained for aforementioned standard images. The standard deviation of the input noise is considered between  $\sigma = 10$  to  $\sigma = 70$ . From the results, it is observed that the proposed 2-D filters perform better in denoising and results are shown in Fig. 4. For clear illustration, we have compared the intensity profiles at 315th row of denoised Barbara image by proposed method with the existing methods along with the noisy image as shown in Fig. 5. From the intensity profiles, it is clear that the proposed method gives superior results. The subband energy distributions of Barbara image is calculated at first-level decomposition for proposed filters and existing filters. The energies of first subband are presented in Table 2. It is clear that proposed filters give better energy compaction as compare to existing methods.

## 5 Conclusion

In this paper, the design of two-dimensional quincunx filterbank has been proposed based on 2-D eigenfilter approach with directional vanishing moment. The proposed filters satisfy the PR criteria and have comparable performance with existing 2-D filters. The performance of the proposed filters has been tested in image denoising applications. In order to obtain insightful analysis, the quantitative measures such as SNR and PSNR have been measured and compared with the existing methods. It has been observed that the proposed filters give notable denoising results.

## References

1. R. Ansari, A. Cetin, S.H. Lee, Sub-band coding of images using nonrectangular filter banks, in *Proceedings SPIE Applications of Digital Image Processing*, vol. 0974 (1988), p. 0974 – 0974 – 9
2. R.H. Bamberger, M.J.T. Smith, A filter bank for the directional decomposition of images: theory and design. *IEEE Trans. Signal Process.* **40**(4), 882–893 (1992)
3. A.E. Cetin, O.N. Gerek, Y. Yardimci, Equiripple FIR filter design by the FFT algorithm. *IEEE Signal Process. Mag.* **14**(2), 60–64 (1997)
4. Y. Chen, M.D. Adams, W.S. Lu, Design of optimal quincunx filter banks for image coding via sequential quadratic programming, in *IEEE International Conference on Acoustics, Speech and Signal Processing - ICASSP '07*, vol. 3 (2007), pp. III–897–III–900
5. C. Cruz, A. Foi, V. Katkovnik, K. Egiazarian, Nonlocality-reinforced convolutional neural networks for image denoising. *IEEE Signal Process. Lett.* **25**(8), 1216–1220 (2018)
6. A.L. da Cunha, M.N. Do, On two-channel filter banks with directional vanishing moments. *IEEE Trans. Image Process.* **16**(5), 1207–1219 (2007)
7. A. Danielyan, V. Katkovnik, K. Egiazarian, BM3D frames and variational image deblurring. *IEEE Trans. Image Process.* **21**(4), 1715–1728 (2012)
8. M.N. Do, M. Vetterli, The contourlet transform: an efficient directional multiresolution image representation. *IEEE Trans. Image Process.* **14**(12), 2091–2106 (2005)
9. R. Eslami, H. Radha, Translation-invariant contourlet transform and its application to image denoising. *IEEE Trans. Image Process.* **15**(11), 3362–3374 (2006)
10. L. Fan, X. Li, H. Fan, Y. Feng, C. Zhang, Adaptive texture-preserving denoising method using gradient histogram and nonlocal self-similarity priors. *IEEE Trans. Circuits Syst. Video Technol.* **29**(11), 3222–3235 (2019)
11. C. Guillemot, A.E. Cetin, R. Ansari, M-channel nonrectangular wavelet representation for 2-D signals: basis for quincunx sampled signals, in *ICASSP 91: International Conference on Acoustics, Speech, and Signal Processing*, vol. 4, (1991), pp. 2813–2816
12. J. Kim, J.K. Lee, K.M. Lee, Accurate image super-resolution using very deep convolutional networks, in *2016 IEEE Conference on Computer Vision and Pattern Recognition (CVPR)* (2016), pp. 1646–1654
13. J. Kovacevic, M. Vetterli, Nonseparable multidimensional perfect reconstruction filter banks and wavelet bases of  $R^n$ . *IEEE Trans. Inf. Theory* **38**(2), 533–555 (1992)
14. X. Li, Y. Hu, X. Gao, D. Tao, B. Ning, A multi-frame image super-resolution method. *Sig. Process.* **90**(2), 405–414 (2010)
15. R. Mersereau, W. Mecklenbrauker, T. Quatieri, McClellan transformation for 2D filtering : I-design. *IEEE Trans. Circuits Syst.* **23**(7), 405–414 (1976)
16. M.B. Nagare, B.D. Patil, R.S. Holambe, Design of two-dimensional quincunx FIR filter banks using eigen filter approach, in *International Conference on Signal and Information Processing (ICONSIP)* (2016), pp. 1–5
17. M.B. Nagare, B.D. Patil, R.S. Holambe, A multi directional perfect reconstruction filter bank designed with 2-D eigenfilter approach: application to ultrasound speckle reduction. *J. Med. Syst.* **41**(2), 31 (2016b)
18. M.B. Nagare, , B.D. Patil, R.S. Holambe, On the design of biorthogonal halfband filterbanks with almost tight rational coefficients. *IEEE Trans. Circuits Syst. II: Express Briefs* 1-11 (2019)



19. S. Nah, T.H. Kim, K.M. Lee, Deep multi-scale convolutional neural network for dynamic scene deblurring, in *2017 IEEE Conference on Computer Vision and Pattern Recognition (CVPR)* (2017), pp. 257–265
20. A.K. Naik, R.S. Holambe, New approach to the design of low complexity 9/7 tap wavelet filters with maximum vanishing moments. *IEEE Trans. Image Process.* **23**(12), 5722–5732 (2014)
21. B.D. Patil, P.G. Patwardhan, V.M. Gadre, Eigenfilter approach to the design of one-dimensional and multidimensional two-channel linear-phase fir perfect reconstruction filter banks. *IEEE Trans. Circuits Syst. I Regul. Pap.* **55**(11), 3542–3551 (2008)
22. S.-C. Pei, J.-J. Shyu, Design of 2D FIR digital filters by McClellan transformation and least squares eigencontour mapping. *IEEE Trans. Circuits Syst. II: Analog Digit. Signal Process.* **40**(9), 546–555 (1993)
23. S.-C. Pei, C.-C. Tseng, W.-S. Yang, FIR filter designs with linear constraints using the eigenfilter approach. *IEEE Trans. Circuits Syst. II: Analog Digit. Signal Process.* **45**(2), 232–237 (1998)
24. E. Psarakis, G. Moustakides, Design of two-dimensional zero-phase FIR filters via the generalized McClellan transform. *IEEE Trans. Circuits Syst.* **38**(11), 1355–1363 (1991)
25. A.D. Rahulkar, R.S. Holambe, *Iris Image Recognition- Wavelet Filter-banks Based Iris Feature Extraction Schemes*. SpringerBriefs in Signal Processing (2014)
26. Standard test images. <https://www.ece.rice.edu/~wakin/images/>
27. A. Tkachenko, P.P. Vaidyanathan, T. Nguyen, On the eigenfilter design method and its applications: a tutorial. *IEEE Trans. Circuits Syst.* **50**, 497–517 (2003)
28. K. Zhang, W. Zuo, L. Zhang, FFDNet: toward a fast and flexible solution for CNN-based image denoising. *IEEE Trans. Image Process.* **27**(9), 4608–4622 (2018)
29. L. Zhang, P. Bao, W. Xiaolin, Multiscale Immse-based image denoising with optimal wavelet selection. *IEEE Trans. Circuits Syst. Video Technol.* **15**(4), 469–481 (2005)

**Publisher's Note** Springer Nature remains neutral with regard to jurisdictional claims in published maps and institutional affiliations.